Global phase insensitive loss function for deep learning in holographic imaging and projection applications

Yijie Zheng[a] and George Gordon[a]

[a]University of Nottingham, Optics and Photonics Research Group, Nottingham, United Kingdom

ABSTRACT

Holographic imaging and projection are increasingly used for important applications such as augmented reality,[1] 3D microscopy[2] and imaging through optical fibres.[3] However, there are emerging applications that require control or detection of phase, where deep learning techniques are used as faster alternatives to conventional hologram generation algorithms or phase-retrieval algorithms.[4] Although conventional mean absolute error (MAE) loss function or mean squared error (MSE) can directly compare complex values for absolute control of phase, there is a class of problems whose solutions are degenerate within a global phase factor, but whose relative phase between pixels must be preserved. In such cases, MAE is not suitable because it is sensitive to global phase differences. We therefore develop a 'global phase insensitive' loss function that estimates the global phase factor between predicted and target outputs and normalises the predicted output to remove this factor before calculating MAE. As a case study we demonstrate $\leq 0.1\%$ error in the recovery of complex-valued optical fibre transmission matrices via a neural network. This global phase insensitive loss function will offer new opportunities for deep learning-based holographic image reconstruction, 3D holographic projection for augmented reality and coherent imaging through optical fibres.

Keywords: Custom loss function; Neural network; Global phase; holographic imaging applications

1. INTRODUCTION

Holographic imaging and projection techniques that utilize light interference show increasing advantages in recording high-resolution images and measurements of tissues and internal organs,[1] including label-free imaging of samples at a low-radiation dose, inference of the objects' phase distribution such as imaging for live cells and other biological specimens within a liquid environment[5].[6] For applications such as 2D displays, only the amplitude/intensity of the light used is relevant. However, emerging applications require control or detection of phase, such as imaging and projection through optical fibres.[7] To control or recover this phase information, traditional approaches have used methods such as iterative phase retrieval, increasing dimensionality or gradient descent.[8] More recently, deep-learning approaches based on neural networks have been applied to achieve phase recovery[9][10][11][12] and also to the related problem of phase unwrapping[13].[14]

Recent developments in the field of deep learning as faster alternatives to conventional hologram generation algorithms[4] have opened up exciting avenues for significantly advancing holography and coherent imaging systems. These problems are generally framed as supervised learning problems, which means that the weights of the neural network are updated in a way that minimizes the error between the network output values and the target values in terms of a defined loss function,[15] where most commonly, the amplitudes of predictions and targets are compared using a mean absolute error (MAE) loss function or mean squared error (MSE). The two standard approaches currently used to deal with phase information are either to discard it completely, as in the case of using holograms to project amplitude images, or to compute MAE between real and imaginary parts, which implicitly learns an arbitrary global phase factor. However, there is a class of problems whose solutions trained by deep learning models degenerate within a global phase factor, but whose relative phase between pixels

Further author information:
Yijie Zheng: E-mail: slyyz1@exmail.nottingham.ac.uk
George Gordon: E-mail: george.gordon@nottingham.ac.uk

must be preserved. In such cases, models may arbitrarily learn a global phase factor (a type of 'overfitting') and may thus not be generalisable.

In this paper, we therefore propose a customized-defined loss function termed a 'global phase insensitive' loss function that can eliminate the effect of global phase factor during the training process by estimating the factor and normalising the predicted output value before calculating MAE. As a case study we demonstrate $\leq 0.1\%$ error in recovering complex-valued optical fibre transmission matrices via a neural network.

2. GLOBAL PHASE INSENSITIVE LOSS FUNCTION

Conventional loss functions such as mean absolute error(MAE) calculate the absolute difference between predicted and target output values but shows limitations in some holographic imaging cases with a global phase factor arising. Figure 1(a) shows one example of a pair of predicted and target matrix with complex entries depicted as vectors. A global phase difference of π has been introduced between the predicted (red) and target (blue) entries. Figure 1(b) shows the complex error between these two matrices when using MAE as the loss function. Due to the global phase shift, we observe that the vectors have large magnitudes, which will lead to an overall very large MAE when their magnitudes are summed. In the limiting case where the predicted and target matrices are identical, this π global phase shift can result in MAE of 100% when the true value should be 0%. To avoid this problem, we propose a custom loss function called 'global phase insensitive' that eliminates this arbitrary global phase factor before calculating the absolute error:

$$L(\boldsymbol{P}, \boldsymbol{T}) = \sum_{n=1}^{m} \left| \boldsymbol{T_n} - \boldsymbol{P_n} e^{1i\phi(\sum \boldsymbol{T_n} \oslash \boldsymbol{P_n})} \right| \tag{1}$$

where,$\boldsymbol{P}$ and $\boldsymbol{T}$ represent predicted and target output value respectively, m represents the number of matrix elements, $\sum$ represents calculating sum for matrix, ϕ represents the argument function for a complex number input, and $\oslash$ represents element-wise division.

Basically, the global phase factor represented by $e^{1i\phi(\sum \boldsymbol{T_n} \oslash \boldsymbol{P_n})}$ is the phase of a complex number representing the sum of the elements of the complex difference matrix between predicted and target matrices. The rationale for this is that the element-wise phase differences may be approximately similar, as shown in Figure 1(c), so when summed will produce an overall vector with the relevant global phase shift, shown in Figure 1(d). This means the predicted output value can be calibrated by multiplying the phase factor to obtain the expected predicted output value that the model then uses to compute further parameter updates in the gradient descent algorithm. It can be seen from figure 1(e), after eliminating the phase factor, the complex error between the predicted and target output value is reduced to a minimum.

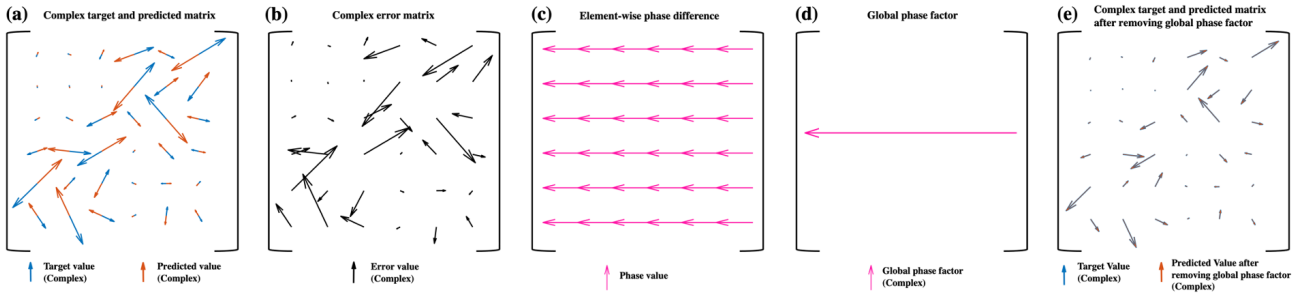

Figure 1. Global phase insensitive loss function
(a) Example of a pair of complex predicted and target output matrix, where blue vectors represent target matrix and red vectors represent predicted matrix, (b) Complex error between predicted and target output matrix, (c) Element-wise phase difference, (d) Global phase factor, (e) Blue vectors represent target matrix and red vectors represent predicted matrix after removing global phase factor

3. CASE STUDY: TRANSMISSION MATRIX RECONSTRUCTION OF SINGLE-ENDED OPTICAL FIBRE SYSTEM

As a case study, we looked at one example of fibre transmission matrix (TM) reconstruction of single-ended optical fibre system using deep learning model, where we placed three-layer reflector stacks that enable single-ended measurement at proximal facet (shown in Figure 2), avoiding practically challenging in clinical use.[3]

Figure 2. Single-ended optical fibre system

$$\boldsymbol{y} = \boldsymbol{A}^T \boldsymbol{R} \boldsymbol{A} \boldsymbol{x} \tag{2}$$

$$\boldsymbol{C} = \boldsymbol{y}\boldsymbol{x}^{-1} = \boldsymbol{A}^T \boldsymbol{R} \boldsymbol{A} \tag{3}$$

where $\boldsymbol{x}$ and $\boldsymbol{y}$ represent input and output field respectively, $\boldsymbol{A}$ represents TM and $\boldsymbol{R}$ represents the reflector matrix.

However, there are no unique solutions $\mathbf{A}$, to Equation3 due to its transpose symmetry properties. Gordon et al. proposed repeating these measurements at 3 wavelengths, giving modified but related transmission matrices, $\boldsymbol{A}$, and different reflector properties, $\boldsymbol{R}$. These three equations can be solved using an iterative approach, but it is computationally slow.[3] Furthermore, the measurement of the fibre's transmission matrix (TM) is required for calibration immediately prior to imaging in a clinical scenario due to its high sensitivity to the bending condition and temperature, and so computational time must be minimised. We have therefore developed a much faster TM recovery model based on Neural Networks (NN).

In terms of TM reconstruction, we generated pairs of data in order for training and validation, including transmission matrix $\boldsymbol{A}$ in Equation3, reflector matrix $\boldsymbol{R}$ in Equation3 and also reflection process matrix $\boldsymbol{C}$ in Equation3. In this case, we simulated reflection process matrix $\boldsymbol{C} \in [12\times12]$ at three different wavelengths ($850nm$, $852nm$ and $854nm$) as the model input and its corresponding transmission matrix $\boldsymbol{A}$ at $850nm$ wavelength as the model output. Figure 3(a) shows one example of generated transmission matrix, where realistic TM gathers the majority of power intensity along the diagonal with additional power spread along the 1^{st} and 2^{nd} sub-diagonals. In order to feed the neural network, both $\boldsymbol{C}$ and $\boldsymbol{A}$ are required to be real-valued matrices. Basically, a 1×1 complex-valued matrix can be described as all real-valued matrix in equation4:

$$a + bi = \begin{bmatrix} a & -b \\ b & a \end{bmatrix} \tag{4}$$

Based on this, in terms of the data preparation for training the deep learning model, Figure 3(b) shows all real-valued $\boldsymbol{A} \in [24\times24]$ and figure 3(c) shows all real-valued $\boldsymbol{C} \in [24\times24]$ after doing data normalization from range -1 and 1.

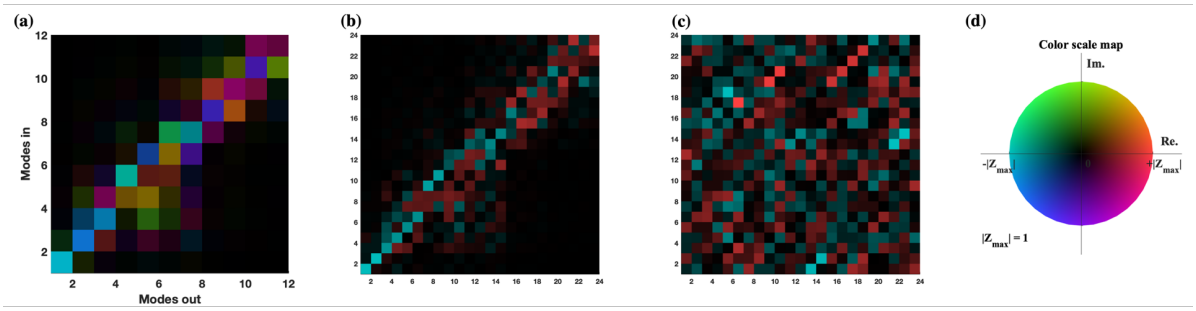

Figure 3. Data preparation for training deep learning models
(a) Example of generated complex-valued transmission matrix $\boldsymbol{A}$, (b) All real-valued TM $\boldsymbol{A}$, (c) All real-valued reflection process matrix $\boldsymbol{C}$, (d) Colormap

3.1 Fully-connected neural network model

We developed a fully connected neural network (FCNN) that used a seven-layer densely connected neural network (five hidden layers), each layer includes 1024 neurons with LeakyRelu activation function. Figure 4 shows the FCNN architecture, where reflection process matrices $\mathbf{C}_1$, $\mathbf{C}_2$ and $\mathbf{C}_3$ at wavelengths of ($850nm$,$852nm$,$854nm$) are concentrated as the input of the model with transmission matrix $\mathbf{A}_1$ at a wavelength of 850 nm as the output. Batch normalization layers and dropout layers at the rate of 0.1 were defined between every dense layer, with two skip connections developed in order to prevent the model being overfitting. The model is trained iteratively with the 'global phase insensitive' custom loss function defined in the previous section. Also, 2500 epochs were used for 60,000 training datasets. The Adam optimiser was used with a learning rate of 0.004 in a decay rate of 1e-4.

The training process was implemented using Tensorflow 2.0 running on a NVIDIA Tesla V100 GPU. MATLAB was used for data pre-processing and post-processing because of its ease-of-use for complex matrix computations.

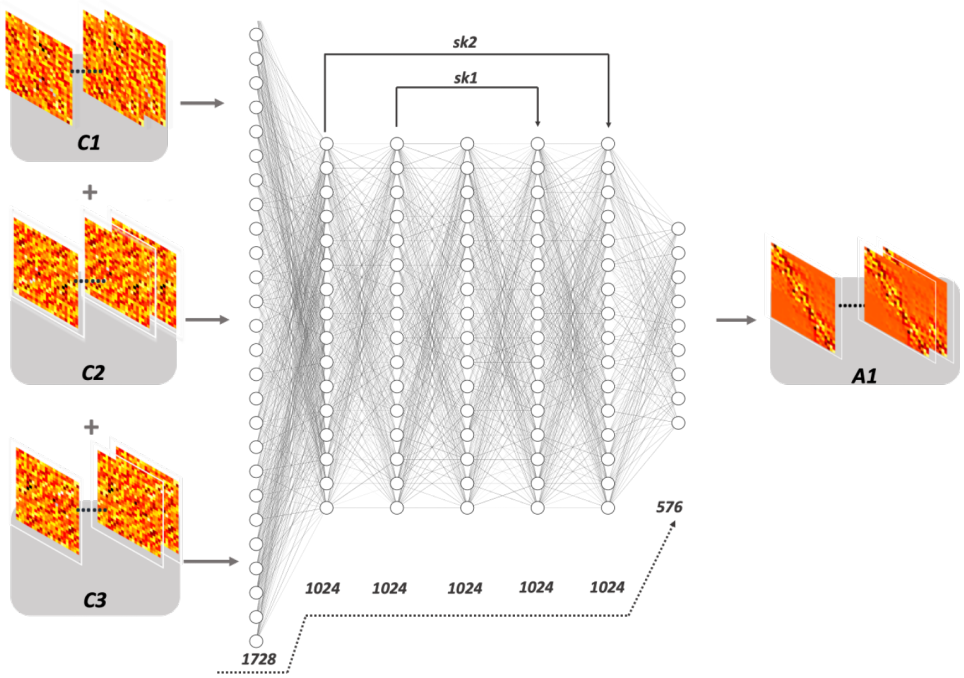

Figure 4. Fully connected neural network (FCNN) architecture

3.2 Validation Result

The model was validated using a subset of the generated dataset that was not used in training. The reconstructed results required convention back to complex-valued matrices for validation. Figure 5 shows one example of a reconstructed result in validation, where 5(a) represents reconstructed TM and 5(b) represents actual TM with the difference shown in 5(c). It can be seen that, reconstructed TM shows relatively low error $\leq 0.1\%$ compared to the actual value both in amplitude and phase and also it reduced the computational running time within $1s$.

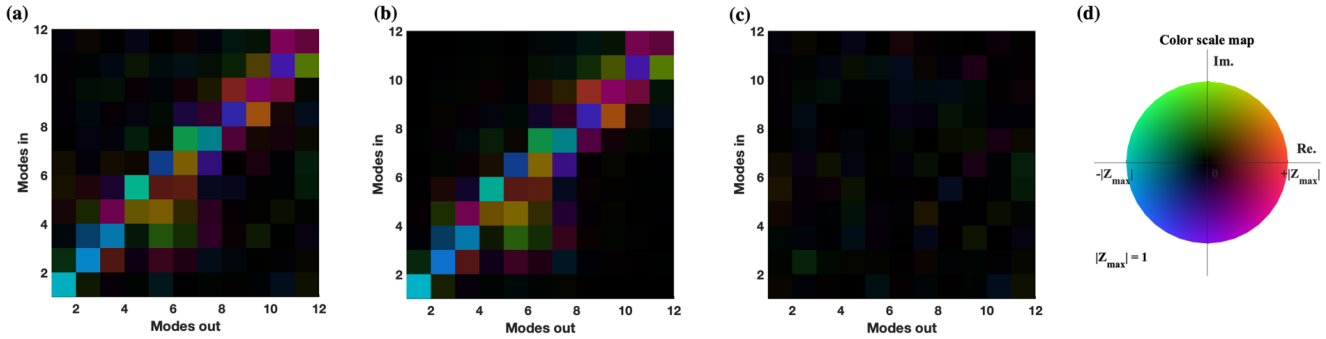

Figure 5. Validation results
(a) Reconstructed transmission matrix $\mathbf{A_R}$, (b) Target transmission matrix $\mathbf{A_T}$, (c) Reconstruction error, (d) Colormap

4. CONCLUSION

In this paper, we proposed a custom loss function that is capable of eliminating the arbitrary global phase factor that arises between predicted and target output values during training of deep-learning models with complex-valued data such as transmission matrices or holograms. We demonstrated this global phase insensitive loss function for a case study of reconstructing 12×12 complex-valued fibre transmission matrices through a single-ended optical fibre system with a $\leq 0.1\%$ error. We anticipate this new loss function will lead to new machine-learning models that deal with phase information, for example in holographic imaging and projection, where both phase control and speed are required.

ACKNOWLEDGMENTS

The authors acknowledge support from a UKRI Future Leaders Fellowship (MR/T041951/1).

REFERENCES

[1] Maimone, A., Georgiou, A., and Kollin, J. S., "Holographic near-eye displays for virtual and augmented reality," *ACM Transactions on Graphics (Tog)* **36**(4), 1–16 (2017).

[2] Wu, Y. and Ozcan, A., "Lensless digital holographic microscopy and its applications in biomedicine and environmental monitoring," *Methods* **136**, 4–16 (2018).

[3] Gordon, G. S., Gataric, M., Ramos, A. G. C., Mouthaan, R., Williams, C., Yoon, J., Wilkinson, T. D., and Bohndiek, S. E., "Characterizing optical fiber transmission matrices using metasurface reflector stacks for lensless imaging without distal access," *Physical Review X* **9**(4), 041050 (2019).

[4] Peng, Y., Choi, S., Padmanaban, N., and Wetzstein, G., "Neural holography with camera-in-the-loop training," *ACM Transactions on Graphics (TOG)* **39**(6), 1–14 (2020).

[5] Bianco, V., Mandracchia, B., Marchesano, V., Pagliarulo, V., Olivieri, F., Coppola, S., Paturzo, M., and Ferraro, P., "Endowing a plain fluidic chip with micro-optics: a holographic microscope slide," *Light: Science & Applications* **6**(9), e17055–e17055 (2017).

[6] Merola, F., Memmolo, P., Miccio, L., Savoia, R., Mugnano, M., Fontana, A., D'ippolito, G., Sardo, A., Iolascon, A., Gambale, A., et al., "Tomographic flow cytometry by digital holography," *Light: Science & Applications* **6**(4), e16241–e16241 (2017).

[7] Mouthaan, R., Christopher, P. J., Pinnell, J., Frosz, M., Gordon, G., Wilkinson, T. D., and Euser, T. G., "Efficient excitation of high-purity modes in arbitrary waveguide geometries," *Journal of Lightwave Technology* **40**(4), 1150–1160 (2022).

[8] Jaganathan, K., Eldar, Y., and Hassibi, B., "Phase retrieval: an overview of recent developments (2015)," *arXiv preprint arXiv:1510.07713* .

[9] Rivenson, Y., Zhang, Y., Günaydın, H., Teng, D., and Ozcan, A., "Phase recovery and holographic image reconstruction using deep learning in neural networks," *Light: Science & Applications* **7**(2), 17141–17141 (2018).

[10] Sinha, A., Lee, J., Li, S., and Barbastathis, G., "Lensless computational imaging through deep learning," *Optica* **4**(9), 1117–1125 (2017).

[11] Wu, Y., Rivenson, Y., Zhang, Y., Wei, Z., Günaydin, H., Lin, X., and Ozcan, A., "Extended depth-of-field in holographic imaging using deep-learning-based autofocusing and phase recovery," *Optica* **5**(6), 704–710 (2018).

[12] Goy, A., Arthur, K., Li, S., and Barbastathis, G., "Low photon count phase retrieval using deep learning," *Physical review letters* **121**(24), 243902 (2018).

[13] Spoorthi, G., Gorthi, S., and Gorthi, R. K. S. S., "Phasenet: A deep convolutional neural network for two-dimensional phase unwrapping," *IEEE Signal Processing Letters* **26**(1), 54–58 (2018).

[14] Dardikman, G. and Shaked, N. T., "Phase unwrapping using residual neural networks," in [*Computational Optical Sensing and Imaging*], CW3B–5, Optica Publishing Group (2018).

[15] Rivenson, Y., Wu, Y., and Ozcan, A., "Deep learning in holography and coherent imaging," *Light: Science & Applications* **8**(1), 1–8 (2019).